Electron Polarimetry with Nonlinear Compton Scattering

Yan-Fei Li,[1] Ren-Tong Guo,[1] Rashid Shaisultanov,[2] Karen Z. Hatsagortsyan,[2] and Jian-Xing Li[1,*]

[1] *MOE Key Laboratory for Nonequilibrium Synthesis and Modulation of Condensed Matter, School of Science, Xi'an Jiaotong University, Xi'an 710049, China*

[2] *Max-Planck-Institut für Kernphysik, Saupfercheckweg 1, 69117 Heidelberg, Germany*

(Received 11 April 2019; revised manuscript received 4 May 2019; published 25 July 2019)

Impacts of spin polarization of an ultrarelativistic electron beam head-on colliding with a strong laser pulse on emitted photon spectra and electron dynamics are investigated in the quantum radiation regime. We simulate photon emissions quantum mechanically and electron dynamics semiclassically via taking spin-resolved radiation probabilities in the local constant field approximation. A small ellipticity of the laser field brings about an asymmetry in the angle-resolved photon spectrum, which sensitively relies on the polarization of the electron beam. The asymmetry is particularly significant in high-energy photon spectra and is employed for the polarization detection of a high-energy electron beam with extraordinary precision, e.g., better than 0.3% for a few-GeV electron beam at a density of the scale of 10^{16} cm^{-3} with currently available strong laser fields. This method demonstrates a method of single-shot determination of polarization for ultrarelativistic electron beams via nonlinear Compton scattering. A similar method based on the asymmetry in the electron momentum distribution after the interaction due to the spin-dependent radiation reaction is proposed as well.

DOI: 10.1103/PhysRevApplied.12.014047

I. INTRODUCTION

Relativistic spin-polarized electron beams are extensively employed in nuclear physics and high-energy physics, e.g., to determine the neutron spin structure [1], to probe nuclear structures [2], to generate polarized photons and positrons [3], to study parity violation [4], and to explore new physics beyond the Standard Model [5]. They are generally produced either via an indirect method, first extracting polarized electrons from a photocathode [6] or spin filters [7–9] and then accelerating them, e.g., via laser wakefield acceleration [10], or via a direct method, transversely polarizing a relativistic electron beam in a storage ring via radiative polarization (the Sokolov-Ternov effect) [11–14]. Relativistic polarized positrons are commonly generated by Compton scattering or bremsstrahlung of circularly polarized lasers and successive pair creation [15,16]. Also, spin rotation systems can be utilized to alter the polarization direction [17].

With rapid developments of strong laser techniques, stable (energy fluctuation of approximately 1%), ultraintense (peak intensity of approximately 10^{22} W/cm^2 and magnetic field of approximately 4×10^5 Tesla), ultrashort (duration of approximately tens of femtoseconds) laser pulses have been generated [18–21]. Spin effects in nonlinear Compton scattering in such strong laser fields have been widely studied [22–26]. Because of the symmetry of the laser fields, the radiative polarization of an electron beam, similar to the Sokolov-Ternov effect, is vanishing in a monochromatic laser field [27] and rather small in the laser pulse [28], but it can be extremely large in a model setup of strong rotating electric fields [29,30]. Recently, the feasibility of significant polarization of an electron beam in currently achievable elliptically polarized (EP) laser pulses has been demonstrated due to spin-dependent radiation reaction (polarization higher than 70% can be reached) [31]. The positrons from pair production can also be highly polarized in a similar setup (polarization up to 90%) [32] or in an asymmetric two-color laser field [33].

The experiments with polarized electrons require a high precision and reliable polarimetry. Currently, the polarimetry for relativistic electron beams employs the following physical principles: Mott scattering [34], Møller scattering [35,36], linear Compton scattering [37], and synchrotron radiation [38,39]. The polarization of relativistic electrons is detected via asymmetries in electron or photon momentum distribution. However, the Mott and Møller polarimeters are only applicable at low energies (<10 MeV) [40,41] and at low currents ($\lesssim$100 μA, due to target heating and subsequent depolarization at higher beam currents) [42–44], respectively, and the Compton polarimeter usually has to collect a large amount ($\gtrsim 10^5$ [45–47]) of laser shots to reach a small statistical uncertainty of approximately 1%, due to low electron-photon collision luminosity. For low-repetition-rate dense ultrarelativistic electron beams, e.g., produced via strong laser pulses [10,31–33]

*jianxing@xjtu.edu.cn

 © 2019 American Physical Society

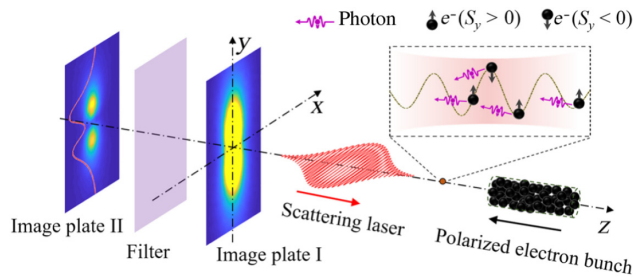

FIG. 1. Scenario of a polarimetry of nonlinear Compton scattering. A strong EP laser pulse, propagating along the $+z$ direction, collides with a transversely polarized (in the y axis) electron bunch. The major axis of the polarization ellipse is along the x axis. The black curve in the subpanel indicates the transverse laser field. Asymmetric angle-resolved spectra of all photons and filtered high-energy photons are shown on Image plate I and Image plate II, respectively.

with an energy of approximately GeV, a total charge of approximately pC, a duration of approximately 10 fs (current $\gtrsim$ 100 A), and a repetition rate (approximately Hz), those first three methods are inapplicable. In addition, their precisions for few-GeV electron beams are typically worse than 0.5% [47–50], which cannot satisfy the stringent request of proposed high-energy experiments, e.g., $\lesssim$ 0.4% [47,51]. The polarimetry with synchrotron radiation is relatively slow (measurement time of approximately 1 s) and not very accurate (precision of approximately 4%) [39], and finally it can be carried out only in a large-scale synchrotron facility. Thus, a more efficient polarimetry with a better precision that is applicable for low-repetition-rate ultrarelativistic electron beams is still a challenge.

In ultraintense laser fields, the Compton scattering would reach the nonlinear realm due to multiphoton absorption [52–54], which could offer new paths for polarimetry, and these paths are especially attractive because of the remarkable increase of the number of emitted photons [55].

In this paper, we theoretically develop an alternative polarimetry method based on nonlinear Compton scattering, which can determine the polarization of a dense ultrarelativistic electron beam via a single-shot interaction with a strong laser pulse, reaching a precision better than 0.3%; see the interaction scenario in Fig. 1. We consider an EP laser pulse of currently available intensity head-on colliding with a polarized ultrarelativistic electron bunch in the quantum radiation regime. Because of the spin dependence of radiation probabilities, the electron most probably emits photons when its spin is antiparallel to the laser magnetic field in its rest frame [chosen as the spin quantization axis (SQA)]. Consequently, the photon emission intensity of the polarized electron beam in adjacent half laser cycles is asymmetric. Moreover, in this specific EP setup, the photons from different half cycles are emitted in opposite directions with respect to the minor polarization axis (y axis) of the laser field, creating an asymmetric angular distribution of radiation; see the detailed explanation below in Fig. 3. Since radiative spin effects are particularly conspicuous for high-energy photons, after filtering, a more visible asymmetric spectrum of high-energy photons shows up, which is exploited for the polarization determination.

II. SIMULATION METHOD

We employ a Monte Carlo method to simulate photon emissions during the electron semiclassical dynamics in an external laser field, which was first developed recently in Ref. [31], based on the spin-resolved quantum radiation probabilities in the local constant field approximation (LCFA). The latter is valid at the invariant laser field parameter $\xi \equiv |e|E_0/(m\omega_0 c) \gg 1$ [54,56], where E_0 and ω_0 are the amplitude and frequency of the laser field, respectively; e and m the electron charge and mass, respectively; and c is the speed of light in vacuum. The radiation probabilities in this regime are characterized by the quantum strong field parameter $\chi \equiv |e|\hbar\sqrt{-(F_{\mu\nu}p^\nu)^2}/m^3c^4$ [54], where $F_{\mu\nu}$ is the field tensor and $\hbar$ the Planck constant. In the employed interaction setup, the electron beam head-on collides with the laser beam, as shown in Fig. 1, and one estimates $\chi \approx 2(\hbar\omega_0/mc^2)\xi\gamma$, with the electron Lorentz γ factor. Q4

The employed radiation probabilities in LCFA are derived with the QED operator method of Baier-Katkov [57] and depend on the electron spin vectors before and after radiation, $\mathbf{S}_i$ and $\mathbf{S}_f$ ($|\mathbf{S}_{i,f}| = 1$) [31,58]. Summing over $\mathbf{S}_f$, the radiation probability depending on the initial spin is obtained (summed up by photon polarization) [57]:

$$\frac{d^2\overline{W}_{\rm fi}}{du d\eta} = 8W_R\big\{-(1+u)\mathrm{Int}K_{13}(u') + (2+2u+u^2)K_{2/3}(u') - u\mathbf{S}_i\cdot\big[\boldsymbol{\beta}\times\hat{\mathbf{a}}\big]K_{1/3}(u')\big\}, \quad (1)$$

where $W_R = \alpha mc/\big[8\sqrt{3}\pi\lambda\!\!\!^{-}_c(k\cdot p_i)(1+u)^3\big]$; $u' = 2u/3\chi$; $u = \omega_\gamma/(\varepsilon_i - \omega_\gamma)$; $\mathrm{Int}K_{1/3}(u') \equiv \int_{u'}^{\infty} dz K_{1/3}(z)$; K_n is the n-order modified Bessel function of the second kind; α the fine structure constant; $\lambda\!\!\!^{-}_c = \hbar/mc$ the Compton wavelength; ω_γ the emitted photon energy; ε_i the electron energy before radiation; $\eta = k\cdot r$ the laser phase; $\boldsymbol{\beta}$ the electron velocity normalized by the speed of light c; p_i, r, and k are the four-vectors of the electron momentum before radiation, coordinate, and laser wave vector, respectively; and $\hat{\mathbf{a}} = \mathbf{a}/|\mathbf{a}|$ with the acceleration $\mathbf{a}$. The widely used radiation probability averaged over the electron spin [59–63] follows from Eq. (1) by setting $\mathbf{S}_i = 0$.

We describe the stochastic radiative spin dynamics in a way following the spirit of the quantum jump approach [64,65]. After a photon emission, the electron spin state is

stochastically collapsed into one of its basis states defined with respect to the instantaneous SQA (along $\boldsymbol{\beta} \times \hat{\mathbf{a}}$); see details in Refs. [31] and [58]. Between photon emissions, the electron dynamics in the external laser field is described by Lorentz equations, and the spin precession is governed by the Thomas-Bargmann-Michel-Telegdi equation [58,66–69].

III. RESULTS AND DISCUSSION

A. Principle of the polarimetry of nonlinear Compton scattering

In the simulations, we use a realistic tightly focused EP laser pulse with a Gaussian temporal profile. The spatial distribution of the electromagnetic fields takes into account up to $(w_0/z_r)^3$ order of the nonparaxial solution [58,70], where w_0 is the laser beam waist size and z_r the Rayleigh length.

Polarization determination via nonlinear Compton scattering is illustrated in Fig. 2. Employed laser and electron beam parameters are the following. The laser peak intensity $I_0 \approx 1.38 \times 10^{22}$ W/cm^2 ($\xi = 100$), wavelength $\lambda_0 = 1$ μm, pulse duration $\tau = 5T_0$, $w_0 = 1.5$ μm, and ellipticity $\epsilon = |E_y|/|E_x| = 0.25$. Such elliptical polarization of ultrastrong laser beams is experimentally achievable; see Refs. [71] and [72]. A cylindrical electron bunch, with radius $w_e = 2\lambda_0$, length $L_e = 15\lambda_0$, and density $n_e \approx 5.3 \times 10^{16}$ cm^{-3}, propagates at a polar angle $\theta_e = 180°$ (with respect to the laser propagation direction) and an azimuthal angle $\phi_e = 0°$ with an angular divergence of 1 mrad. The electron density has a transversely Gaussian and longitudinally uniform distribution. The electron initial kinetic energy is $\varepsilon_0 = 1$ GeV and the energy spread $\Delta\varepsilon_0/\varepsilon_0 = 0.06$. This kind of electron bunch can be achieved by laser wakefield acceleration [73,74] and polarized via radiative spin effects [31–33]. In these conditions, $\chi_{\max} \approx 0.4$ and the pair production can be neglected. Note that the case of relatively low-density electron bunches produced by conventional accelerators or storage rings is also applicable [58].

Figure 2(a) demonstrates an asymmetric angle-resolved spectrum for high-energy photons $\omega_\gamma > 0.1\varepsilon_0$. The asymmetry is more visible in the spectrum integrated over θ_x; see Fig. 2(b). The spectra for $\overline{S}_y = \pm 1$ cases are the most asymmetric and other cases of $-1 < \overline{S}_y < 1$ would appear between them. For the quantitative characterization of asymmetry, we introduce the differential asymmetry parameter $\mathcal{D} = (d\tilde{\varepsilon}_\gamma^+/d\theta_y - d\tilde{\varepsilon}_\gamma^-/d\theta_y)/(d\tilde{\varepsilon}_\gamma^+/d\theta_y + d\tilde{\varepsilon}_\gamma^-/d\theta_y)$, between the values of $d\tilde{\varepsilon}_\gamma/d\theta_y$ at $\theta_y > 0$ (+) and $\theta_y < 0$ (−) with the same $|\theta_y|$, respectively, and the asymmetry parameter $\mathcal{A} = (\widetilde{\mathcal{E}_\gamma}^+ - \widetilde{\mathcal{E}_\gamma}^-)/(\widetilde{\mathcal{E}_\gamma}^+ + \widetilde{\mathcal{E}_\gamma}^-)$, with $\widetilde{\mathcal{E}_\gamma}^+ = \int_{\theta_{\min}}^{\theta_{\max}} (d\tilde{\varepsilon}_\gamma/d\theta_y) d\theta_y$ and $\widetilde{\mathcal{E}_\gamma}^- = \int_{-\theta_{\max}}^{-\theta_{\min}} (d\tilde{\varepsilon}_\gamma/d\theta_y) d\theta_y$. Also, $\theta_{\min} = 2.5$ mrad and $\theta_{\max} = 10$ mrad. The differential asymmetry $\mathcal{D}$ is shown

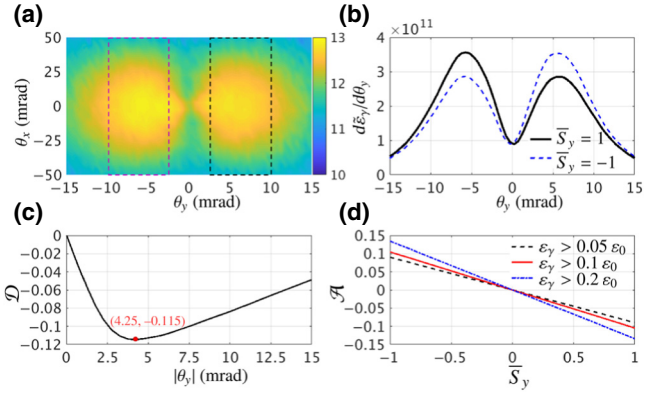

FIG. 2. (a) Angle-resolved spectrum of selected high-energy photons ($\omega_\gamma > 0.1\varepsilon_0$): $\log_{10}[d^2\varepsilon_\gamma/(mc^2 d\theta_x d\theta_y)]$ (rad^{-2}) vs the transverse deflection angles $\theta_x = \arctan(p_x/p_z)$ and $\theta_y = \arctan(p_y/p_z)$, with the initial average polarization $\overline{S}_y = 1$. (b) $d\tilde{\varepsilon}_\gamma/d\theta_y = \int d^2\varepsilon_\gamma/(mc^2 d\theta_x d\theta_y) d\theta_x$ vs θ_y, with $\overline{S}_y = 1$ (black solid curves) and $\overline{S}_y = -1$ (blue dashed), respectively. (c) Differential asymmetry $\mathcal{D}$ for the case of $\overline{S}_y = 1$. (d) Asymmetry $\mathcal{A}$ vs $\overline{S}_y$. The photons used to calculate $\mathcal{A}$ are shown in the boxes in (a). The laser and electron beam parameters are given in the text.

in Fig. 2(c). As $|\theta_y|$ rises from 0 to 15 mrad, $|\mathcal{D}|$ first increases rapidly, reaches the peak of about 11.5% at $|\theta_y| = 4.25$ mrad, and then decreases slowly to 5%. For the asymmetry $\mathcal{A}$, the photons are selected in the regions of $-\theta_{\max} \le \theta_y \le -\theta_{\min}$ and $\theta_{\min} \le \theta_y \le \theta_{\max}$, where $\mathcal{D}$ is apparently large. This angular region exceeds the uncertainty angle of the electron beam $\theta_{\text{uncert}} \sim 1/\gamma \approx 0.7$ mrad [58], as well as the currently achievable angular resolution for gamma-ray detection (< 1 mrad) [75,76].

The asymmetry parameter $\mathcal{A}$ is well suited to determine the polarization; see Fig. 2(d). As $\overline{S}_y$ continuously increases from −1 to 1, $\mathcal{A}$ monotonously decreases from 0.103 to −0.103 for the case of $\omega_\gamma > 0.1\varepsilon_0$. As the chosen photon energy decreases (increases) to $\omega_\gamma > 0.05\varepsilon_0$ ($0.2\varepsilon_0$), the slope of $\mathcal{A}$ curve decreases (increases) as well, with $\mathcal{A}_{\max} = 0.09$ (0.134), which surpasses the asymmetry of the Compton polarimeter (< 0.05) [45–47]. The precision of the polarization measurement can be estimated via the statistical uncertainty $\delta\mathcal{A}/\mathcal{A} \approx 1/\mathcal{A}\sqrt{N_\gamma}$ [77], reaching about 0.265%, 0.31%, and 0.372% for the cases of $\omega_\gamma > 0.05\varepsilon_0$, $0.1\varepsilon_0$, and $0.2\varepsilon_0$, respectively, with the gamma-photon number $N_\gamma \approx 1.75 \times 10^7$, 1×10^7, and 0.4×10^7, respectively, in our simulations. In the case of considering all photons, $\mathcal{A}_{\max} = 0.078$ and the precision is about 0.16%, with $N_\gamma \approx 6.87 \times 10^7$ [58]. However, the experimental systematic uncertainty is inversely proportional to $\mathcal{A}$ [49], which requires a large $\mathcal{A}$.

Note that the polarimetry can also be developed via using the asymmetry of the angular distribution of the photon number, rather than photon energy in Fig. 2, however, with a bit smaller $\mathcal{A}_{\max}$ [58].

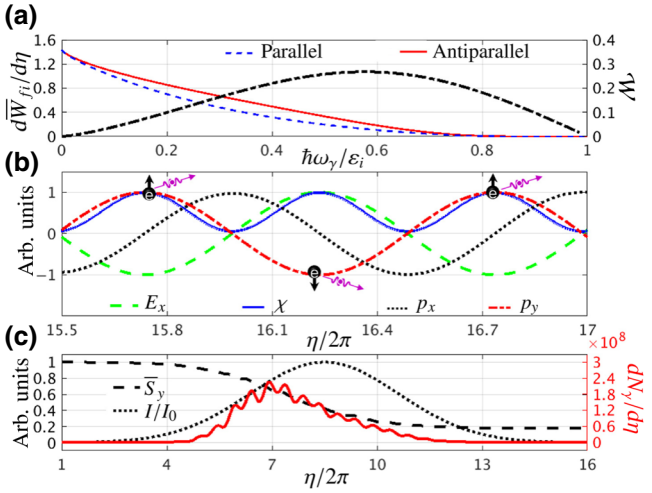

FIG. 3. (a) Photon emission probabilities, $d\overline{W}_{\rm fi}/d\eta$, with the spin vector parallel (blue dashed curve) and antiparallel (red solid) to the instantaneous SQA, respectively, and their relative difference $\mathcal{W} \equiv (d\overline{W}_{\rm fi}^{\rm anti}/d\eta - d\overline{W}_{\rm fi}^{\rm paral}/d\eta)/(d\overline{W}_{\rm fi}^{\rm anti}/d\eta + d\overline{W}_{\rm fi}^{\rm paral}/d\eta)$ (black dashed-dotted) vs $\omega_\gamma/\varepsilon_i$. (b) Variations of E_x (green dashed curve), χ (blue solid), and the p_x (black dotted) and p_y (red dashed-dotted) components of electron momenta, normalized by their maximal values in arbitrary units, with respect to η. (c) Normalized laser pulse intensity (black dotted curve), $\overline{S}_y$ (black dashed), and photon number density (red solid) vs η. The laser and electron beam parameters in (a) and (c) are the same as those in Fig. 2 with $\omega_\gamma > 0.1\varepsilon_0$.

B. Physical interpretation

The reasons for the appearance of asymmetric spectra are analyzed in Fig. 3. In Eq. (1), as the electron spin $\mathbf{S}_i$ is antiparallel to the instantaneous SQA (along $\boldsymbol{\beta} \times \hat{\mathbf{a}}$), the photon emission probability is the largest and apparently larger than the parallel case; see Fig. 3(a). The relative difference of probabilities $\mathcal{W}$ is remarkable for high-energy photons and reaches the peak, about 28%, at $\omega_\gamma \approx 0.6\varepsilon_i$. Thus, the asymmetry of high-energy photons is more visible, as indicated in Fig. 2(d). However, there are many fewer high-energy photons, since the radiation probability declines gradually with the increase of ω_γ. Consequently, an appropriate photon energy ω_γ should be chosen; e.g., in Fig. 2(d), the precision in $\omega_\gamma > 0.05\varepsilon_i$ case is the best.

As demonstrated in Fig. 3(b), for the left-handed laser pulse, E_x has a $\pi/2$ phase delay with respect to E_y. The electron transverse momentum in the laser field $\mathbf{p}_\perp = -e\mathbf{A}(\eta)$, with the vector potential $\mathbf{A}(\eta)$, is ahead by $\pi/2$ with respect to the field $\mathbf{E}(\eta)$. Thus, compared with E_x (green dashed curve), p_x (black dotted) is ahead by $\pi/2$ and p_y (red dashed-dotted) is ahead by π. The radiation probability is determined by $\chi \propto \gamma\xi \propto E_x$. In the half cycles of $E_x > 0$, the SQA is along $\boldsymbol{\beta} \times \hat{\mathbf{a}} \propto e\boldsymbol{\beta} \times \mathbf{E}$, i.e., the $+y$ direction, and consequently, the spin-down (with respect to the $+y$ direction) electrons more probably emit photons, whose p_y are certainly negative, but p_x are uncertain. In $E_x < 0$, the SQA is along the $-y$ direction, and the spin-up electrons more probably emit photons, whose p_y are certainly positive. Thus, an asymmetric spectrum can appear along the y axis for the EP laser pulse, but not for the linearly polarized (LP) case. For the circularly polarized (CP) case, the SQA rotates, the p_y and p_x components of emitted photons are both uncertain, and consequently, the spectrum is symmetric in the x-y plane.

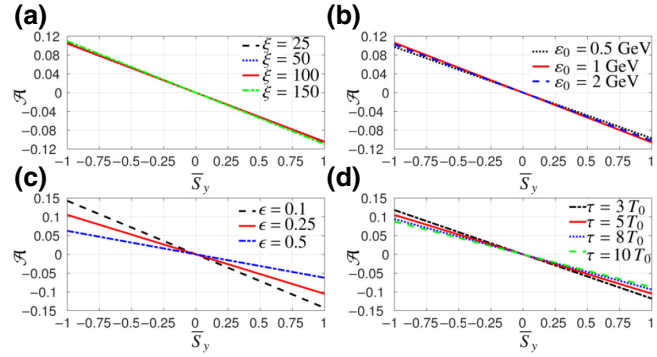

FIG. 4. (a)–(d) Impact of ξ, ε_0, ϵ, and τ on the asymmetry parameter $\mathcal{A}$. In (b), for the cases of $\varepsilon_0 = 0.5$ and 2 GeV, the detection θ_y ranges are 5 mrad $< |\theta_y| <$ 12.5 mrad and 1.25 mrad $< |\theta_y| <$ 8.75 mrad, respectively. In (c), for the cases of $\epsilon = 0.1$ and 0.5, 1 mrad $< |\theta_y| <$ 8.5 mrad and 5 mrad $< |\theta_y| <$ 12.5 mrad, respectively. Other parameters are the same as those in Fig. 2.

Because of radiative stochastic spin flips, the polarization of the electron beam is depressed during propagation through the laser pulse [see Fig. 3(c)], which could weaken the considered asymmetry. For ultrashort laser pulses, the chosen high-energy photons are mainly emitted at the front edge of the pulse, where the beam initial polarization is maintained well, and the asymmetric spectrum corresponds to the initial polarization. However, the asymmetric spectrum of low-energy ($\omega_\gamma \ll \varepsilon_0$) photons, which are still substantially emitted at the back edge of the pulse, can be significantly altered due to the beam depolarization.

Furthermore, we analyze the cases of larger energy spread $\Delta\varepsilon_0/\varepsilon_0 = 0.1$, larger angular divergence of 2 mrad, different collision angles $\theta_e = 179^\circ$ and $\phi_e = 90^\circ$, 2% fluctuation of laser intensity, and the pulse noises. All show stable and uniform results [58]. We underline that radiation reaction effects are not crucial for generating the asymmetry in photon spectra [58].

C. Impact of the laser and electron beam parameters on the polarimetry

We investigate the impact of the laser and electron beam parameters on the polarimetry in Fig. 4. First, as the laser intensity rises, e.g., ξ increases from 25 to 150 in Fig. 4(a), not only the yield of high-energy photons

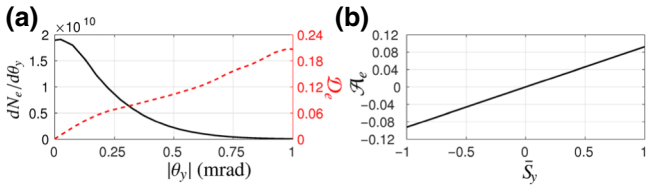

FIG. 5. Polarization determination by the electron momentum distribution asymmetry. (a) $dN_e/d\theta_y$ (rad^{-1}) (black solid curve) and $\mathcal{D}_e$ (red dashed) vs θ_y with $\bar{S}_y = 1$. The calculation of $\mathcal{D}_e$ is the same as $\mathcal{D}$ in Fig. 2 except replacing ε_γ with N_e. (b) The asymmetry parameter, $\mathcal{A}_e = (\tilde{N}_e^{\,+} - \tilde{N}_e^{\,-})/(\tilde{N}_e^{\,+} + \tilde{N}_e^{\,-})$, with respect to $\bar{S}_y$. $\tilde{N}_e^{\,+} = \int_{\theta_{\min}}^{\theta_{\max}} (dN_e/d\theta_y) d\theta_y$ and $\tilde{N}_e^{\,-} = \int_{-\theta_{\max}}^{-\theta_{\min}} (dN_e/d\theta_y) d\theta_y$. $\theta_{\min} = 0.25$ mrad and $\theta_{\max} = 1$ mrad. $\xi = 20$, $\tau = 20T_0$, $\epsilon = 0.1$, $w_0 = 2\lambda_0$, $\varepsilon_0 = 4$ GeV, the electron beam divergence is 0.3 mrad, and other parameters are the same as those in Fig. 2.

increases, but the depolarization effect is also enhanced [58]. Consequently, the $\mathcal{A}$ curve stays stable. The conditions of quantum regime $\chi \approx 2(\hbar\omega_0/mc^2)\xi\gamma \gtrsim 1$ and having a large amount of photons $N_\gamma \sim N_e\alpha\xi\tau/T_0 \gg N_e$ restrict the lower limit of ξ. N_e is the electron number. As $\xi \gg 1$ and $\chi \gg 1$, the pair production and even cascade have to be considered, which would seriously affect high-energy photon spectra. As ε_0 increases, e.g., from 0.5 to 2 GeV in Fig. 4(b), the deflection angle of photons and the uncertainty angle of the electron beam both decrease. The corresponding detection angle ranges have to be adjusted to include the majority of high-energy photons and exceed θ_{uncert}, and the $\mathcal{A}$ curve changes slightly. The photon deflection angle $\theta_y \sim p_y/p_z \propto E_y \propto \epsilon$. As ϵ rises, e.g., from 0.1 to 0.5 in Fig. 4(c), θ_y rises as well, but the rotation effect of SQA in the x-y plane is enhanced (cf. the ultimate case of the CP laser), and consequently, the depolarization effect is enhanced as well. As ϵ is too small (cf. the ultimate case of the LP laser), the photons mix together, and the asymmetry is weakened and even removed. As the laser pulse duration increases, e.g., from $3T_0$ to $10T_0$ (currently achievable cases) in Fig. 4(d), $\mathcal{A}_{\max}$ decreases, since the beam polarization declines due to radiative spin effects, as demonstrated in Fig. 3(c).

D. Polarization determination via the electron momentum distribution

We point out that a similar method of polarimetry can be suggested via the electron momentum distribution asymmetry in the same EP laser setup; see Fig. 5. About 26% of electrons, which are in the range from 0.25 to 1 mrad, exceeding the uncertainty angle θ_{uncert}, are used. $\mathcal{A}_{e,\max} \approx 0.092$ and the precision is about 0.67%. Compared with the above method, this method gives a lower precision, because the considered electron number is smaller than the emitted photon number due to multiple photon emissions as $\xi \gg 1$, but it is more efficient for low laser intensities when $N_\gamma/N_e \sim \alpha\xi\tau/T_0 \lesssim 1$.

Note that our polarimetry method is not noninvasive. The polarization measurement of the electron bunch results in its depolarization and energy broadening [58].

IV. CONCLUSION

We develop an alternative method of polarimetry based on nonlinear Compton scattering in the quantum radiation regime. The electron beam polarization can be measured via the angular asymmetry of the high-energy gamma-photon spectrum in a single-shot interaction of the electron beam with an EP strong laser pulse of currently achievable intensity. The precision for the polarization measurement is better than 0.3% for dense few-GeV electron beams.

ACKNOWLEDGMENTS

This work is supported by the National Natural Science Foundation of China (Grants No. 11874295 and No. 11804269), the Science Challenge Project of China (Grant No. TZ2016099), and the National Key Research and Development Program of China (Grant No. 2018YFA0404801).

[1] P. L. Anthony *et al.*, Determination of the Neutron Spin Structure Function, Phys. Rev. Lett. **71**, 959 (1993).
[2] K. Abe, T. Akagi, P. L. Anthony, R. Antonov, R. G. Arnold, T. Averett, H. R. Band, J. M. Bauer, H. Borel, P. E. Bosted, and V. Breton, Precision Measurement of the Deuteron Spin Structure Function g_1^d, Phys. Rev. Lett. **75**, 25 (1995).
[3] Haakon Olsen and L. C. Maximon, Photon and electron polarization in high-energy bremsstrahlung and pair production with screening, Phys. Rev. **114**, 887 (1959).
[4] D. Androić *et al.* (The Jefferson Lab Q_{weak} Collaboration), Precision measurement of the weak charge of the proton, Nature **557**, 207 (2018).
[5] G. Moortgat-Pick *et al.*, Polarized positrons and electrons at the linear collider, Phys. Rep. **460**, 131 (2008).
[6] Daniel T. Pierce and Felix Meier, Photoemission of spin-polarized electrons from GaAs, Phys. Rev. B **13**, 5484 (1976).
[7] H. Batelaan, A. S. Green, B. A. Hitt, and T. J. Gay, Optically Pumped Electron Spin Filter, Phys. Rev. Lett. **82**, 4216 (1999).
[8] Matthias M. Dellweg and Carsten Müller, Spin-polarizing Interferometric Beam Splitter for Free Electrons, Phys. Rev. Lett. **118**, 070403 (2017).
[9] Matthias M. Dellweg and Carsten Müller, Controlling electron spin dynamics in bichromatic kapitza-dirac scattering by the laser field polarization, Phys. Rev. A **95**, 042124 (2017).
[10] Meng Wen, Matteo Tamburini, and Christoph H. Keitel, Polarized laser-wakefield-accelerated kiloampere electron beams, arXiv:1809.10570 (2018).

[11] A. A. Sokolov and I. M. Ternov, *Synchrotron Radiation* (Akademic, Germany, 1968).

[12] V. N. Baier and V. M. Katkov, Radiational polarization of electrons in inhomogeneous magnetic field, Phys. Lett. A **24**, 327 (1967).

[13] V. N. Baier, Radiative polarization of electrons in storage rings, Sov. Phys. Usp. **14**, 695 (1972).

[14] Y. Derbenev and A. M. Kondratenko, Polarization kinematics of particles in storage rings, Zh. Èksper. Teoret. Fiz. **64**, 1918 (1973).

[15] T. Omori, M. Fukuda, T. Hirose, Y. Kurihara, R. Kuroda, M. Nomura, A. Ohashi, T. Okugi, K. Sakaue, T. Saito, J. Urakawa, M. Washio, and I. Yamazaki, Efficient Propagation of Polarization from Laser Photons to Positrons through Compton Scattering and Electron-positron Pair Creation, Phys. Rev. Lett. **96**, 114801 (2006).

[16] D. Abbott *et al.* (PEPPo Collaboration), Production of Highly Polarized Positrons Using Polarized Electrons at MeV Energies, Phys. Rev. Lett. **116**, 214801 (2016).

[17] J. Buon and K. Steffen, HERA variable-energy "mini" spin rotator and head-on EP collision scheme with choice of electron helicity, Nucl. Instrum. Methods Phys. Res., Sect. A **245**, 248 (1986).

[18] The Vulcan facility, http://www.clf.stfc.ac.uk/Pages/The-Vulcan-10-Petawatt-Project.aspx.

[19] The Extreme Light Infrastructure (ELI), http://www.eli-beams.eu/en/facility/lasers/.

[20] Exawatt Center for Extreme Light Studies (XCELS), http://www.xcels.iapras.ru/.

[21] V. Yanovsky, V. Chvykov, G. Kalinchenko, P. Rousseau, T. Planchon, T. Matsuoka, A. Maksimchuk, J. Nees, G. Cheriaux, G. Mourou, and K. Krushelnick, Ultra-high intensity- 300-Tw laser at 0.1 Hz repetition rate, Opt. Express **16**, 2109 (2008).

[22] P. Panek, J. Z. Kamiński, and F. Ehlotzky, Laser-induced Compton scattering at relativistically high radiation powers, Phys. Rev. A **65**, 022712 (2002).

[23] G. L. Kotkin, V. G. Serbo, and V. I. Telnov, Electron (positron) beam polarization by Compton scattering on circularly polarized laser photons, Phys. Rev. ST Accel. Beams **6**, 011001 (2003).

[24] Dmitry V. Karlovets, Radiative polarization of electrons in a strong laser wave, Phys. Rev. A **84**, 062116 (2011).

[25] Madalina Boca, Victor Dinu, and Viorica Florescu, Spin effects in nonlinear Compton scattering in a plane-wave laser pulse, Nucl. Instrum. Methods Phys. Res., Sect. B **279**, 12 (2012).

[26] K. Krajewska and J. Z. Kamiński, Spin effects in nonlinear Compton scattering in ultrashort linearly-polarized laser pulses, Laser Part. Beams **31**, 503 (2013).

[27] D. Yu. Ivanov, G. L. Kotkin, and V. G. Serbo, Complete description of polarization effects in emission of a photon by an electron in the field of a strong laser wave, Eur. Phys. J. C **36**, 127 (2004).

[28] D. Seipt, D. Del Sorbo, C. P. Ridgers, and A. G. R. Thomas, Theory of radiative electron polarization in strong laser fields, Phys. Rev. A **98**, 023417 (2018).

[29] D. Del Sorbo, D. Seipt, T. G. Blackburn, A. G. R. Thomas, C. D. Murphy, J. G. Kirk, and C. P. Ridgers, Spin polarization of electrons by ultraintense lasers, Phys. Rev. A **96**, 043407 (2017).

[30] D. Del Sorbo, D. Seipt, A. G. R. Thomas, and C. P. Ridgers, Electron spin polarization in realistic trajectories around the magnetic node of two counter-propagating, circularly polarized, ultra-intense lasers, Plasma Phys. Control. Fusion **60**, 064003 (2018).

[31] Yan-Fei Li, Rashid Shaisultanov, Karen Z. Hatsagortsyan, Feng Wan, Christoph H. Keitel, and Jian-Xing Li, Ultrarelativistic Electron-beam Polarization in Single-shot Interaction with an Ultraintense Laser Pulse, Phys. Rev. Lett. **122**, 154801 (2019).

[32] Feng Wan, Rashid Shaisultanov, Yan-Fei Li, Karen Z. Hatsagortsyan, Christoph H. Keitel, and Jian-Xing Li, Ultrarelativistic polarized positron jets via collision of electron and ultraintense laser beams, arXiv:1904.04305 (2019).

[33] Yue-Yue Chen, Pei-Lun He, Rashid Shaisultanov, Karen Z. Hatsagortsyan, and Christoph H. Keitel, Polarized positron beams via intense two-color laser pulses, arXiv:1904.04110 (2019).

[34] N. F. Mott, The scattering of fast electrons by atomic nuclei, Proc. Roy. Soc. (London) **124**, 425 (1929).

[35] C. Møller, On the theory of the passage of rapid electrons through matter, Ann. Phys. **14**, 531 (1932).

[36] P. S. Cooper, M. J. Alguard, R. D. Ehrlich, V. W. Hughes, H. Kobayakawa, J. S. Ladish, M. S. Lubell, N. Sasao, K. P. Schüler, P. A. Souder, G. Baum, W. Raith, K. Kondo, D. H. Coward, R. H. Miller, C. Y. Prescott, D. J. Sherden, and C. K. Sinclair, Polarized Electron-electron Scattering at GeV Energies, Phys. Rev. Lett. **34**, 1589 (1975).

[37] O. Klein and Y. Nishina, Überber die streuung von strahlung durch freie elektronen nach der neuen relativistischen quantendynamik von dirac, Z. Phys. **52**, 853 (1929).

[38] D. P. Barber, H. D. Bremer, M. Böge, R. Brinkmann, W. Brückner, C. Büscher, M. Chapman, K. Coulter, P. P. J. Delheij, Düren, M., Gianfelice-Wendt, E.,, The HERA polarimeter and the first observation of electron spin polarization at HERA, Nucl. Instrum. Methods Phys. Res., Sect. A **329**, 79 (1993).

[39] S. A. Belomesthnykh, A. E. Bondar, M. N. Yegorychev, V. N. Zhilitch, G. A. Kornyukhin, S. A. Nikitin, E. L. Saldin, A. N. Skrinsky, and G. M. Tumaikin, An observation of the spin dependence of synchrotron radiation intensity, Nucl. Instrum. Methods Phys. Res., Sect. A **227**, 173 (1984).

[40] T. J. Gay and F. B. Dunning, Mott electron polarimetry, Rev. Sci. Instrum. **63**, 1635 (1992).

[41] V. Tioukine, K. Aulenbacher, and E. Riehn, A Mott polarimeter operating at mev electron beam energies, Rev. Sci. Instrum. **82**, 033303 (2011).

[42] D. Gaskell, D. G. Meekins, and C. Yan, New methods for precision Møller polarimetry? Eur. Phys. J. A **32**, 561 (2007).

[43] M. Hauger, A. Honegger, J. Jourdan, G. Kubon, T. Petitjean, D. Rohe, I. Sick, G. Warren, H. Wöhrle, J. Zhao, R. Ent, J. Mitchell, D. Crabb, A. Tobias, M. Zeier, and B. Zihlmann, A high-precision polarimeter, Nucl. Instrum. Methods Phys. Res., Sect. A **462**, 382 (2001).

[44] Kurt Aulenbacher, Eugene Chudakov, David Gaskell, Joseph Grames, and Kent D. Paschke, Precision electron beam polarimetry for next generation nuclear physics experiments, Int. J. Mod. Phys. E **27**, 1830004 (2018).

[45] M. Beckmann, A. Borissov, S. Brauksiepe, F. Burkart, H. Fischer, J. Franz, F. H. Heinsius, K. Königsmann, W. Lorenzon, F. M. Menden, A. Most, S. Rudnitsky, C. Schill, J. Seibert, and A. Simon, The longitudinal polarimeter at HERA, Nucl. Instrum. Methods Phys. Res., Sect. A **479**, 334 (2002).

[46] S. Escoffier, P. Y. Bertin, M. Brossard, E. Burtin, C. Cavata, N. Colombel, C. W. de Jager, A. Delbart, D. Lhuillier, F. Marie, J. Mitchell, D. Neyret, and T. Pussieux, Accurate measurement of the electron beam polarization in JLab hall a using compton polarimetry, Nucl. Instrum. Methods Phys. Res., Sect. A **551**, 563 (2005).

[47] A. Narayan *et al.*, Precision Electron-beam Polarimetry at 1 GeV Using Diamond Microstrip Detectors, Phys. Rev. X **6**, 011013 (2016).

[48] K. Abe *et al.* (SLD Collaborationion), High-precision Measurement of the Left-right *Z* Boson Cross-section Asymmetry, Phys. Rev. Lett. **84**, 5945 (2000).

[49] M. Friend, D. Parno, F. Benmokhtar, A. Camsonne, M. M. Dalton, G. B. Franklin, V. Mamyan, R. Michaels, S. Nanda, V. Nelyubin, K. Paschke, B. Quinn, A. Rakhman, P. Souder, and A. Tobias, Upgraded photon calorimeter with integrating readout for the hall a compton polarimeter at Jefferson lab, Nucl. Instrum. Methods Phys. Res., Sect. A **676**, 96 (2012).

[50] M. Hauger, A. Honegger, J. Jourdan, G. Kubon, T. Petitjean, D. Rohe, I. Sick, G. Warren, H. Wöhrle, J. Zhao, R. Ent, J. Mitchell, D. Crabb, A. Tobias, M. Zeier, and B. Zihlmann, A high-precision polarimeter, Nucl. Instrum. Methods Phys. Res., Sect. A **462**, 382 (2001).

[51] J. Benesch *et al.*, The moller experiment: An ultra-precise measurement of the weak mixing angle using Møller scattering, arXiv:1411.4088 (2014).

[52] I. I. Gol'dman, Intensity effects in compton scattering, Sov. Phys. JETP **19**, 954 (1964), [Zh. Eksp. Teor. Fiz. **46**, 1412 (1964)].

[53] A. I. Nikishov and V. I. Ritus, Quantum processes in the field of a plane electromagnetic wave and in a constant field. I, Sov. Phys. JETP **19**, 529 (1964), [Zh. Eksp. Teor. Fiz. **46**, 776 (1964)].

[54] V. I. Ritus, Quantum effects of the interaction of elementary particles with an intense electromagnetic field, J. Sov. Laser Res. **6**, 497 (1985).

[55] A. Di Piazza, C. Müller, K. Z. Hatsagortsyan, and C. H. Keitel, Extremely high-intensity laser interactions with fundamental quantum systems, Rev. Mod. Phys. **84**, 1177 (2012).

[56] V. N. Baier, V. M. Katkov, and V. M. Strakhovenko, *Electromagnetic Processes at High Energies in Oriented Single Crystals* (World Scientific, Singapore, 1998).

[57] V. N. Baier, V. M. Katkov, and V. S. Fadin, *Radiation from Relativistic Electrons* (Atomizdat, Moscow, 1973).

[58] See Supplemental Material at http://link.aps.org/supplemental/10.1103/PhysRevApplied.12.014047 for details on the employed laser fields, on the applied theoretical model, on the simulation results for other laser or electron parameters, and on the polarization determination by the electron momentum distribution.

[59] Igor V. Sokolov, John A. Nees, Victor P. Yanovsky, Natalia M. Naumova, and Gérard A. Mourou, Emission and its back-reaction accompanying electron motion in relativistically strong and QED-strong pulsed laser fields, Phys. Rev. E **81**, 036412 (2010).

[60] N. V. Elkina, A. M. Fedotov, I. Yu. Kostyukov, M. V. Legkov, N. B. Narozhny, E. N. Nerush, and H. Ruhl, QED cascades induced by circularly polarized laser fields, Phys. Rev. ST Accel. Beams **14**, 054401 (2011).

[61] C. P. Ridgers, J. G. Kirk, R. Duclous, T. G. Blackburn, C. S. Brady, K. Bennett, T. D. Arber, and A. R. Bell, Modelling gamma-ray photon emission and pair production in high-intensity laser–matter interactions, J. Comput. Phys. **260**, 273 (2014).

[62] D. G. Green and C. N. Harvey, SIMLA: Simulating particle dynamics in intense laser and other electromagnetic fields via classical and quantum electrodynamics, Comput. Phys. Commun. **192**, 313 (2015).

[63] C. N. Harvey, A. Ilderton, and B. King, Testing numerical implementations of strong-field electrodynamics, Phys. Rev. A **91**, 013822 (2015).

[64] Klaus Mølmer and Yvan Castin, Monte carlo wavefunctions in quantum optics, Quantum Semiclass. Opt. **8**, 49 (1996).

[65] M. B. Plenio and P. L. Knight, The quantum-jump approach to dissipative dynamics in quantum optics, Rev. Mod. Phys. **70**, 101 (1998).

[66] L. H. Thomas, The motion of the spinning electron, Nature (London) **117**, 514 (1926).

[67] L. H. Thomas, The kinematics of an electron with an axis, Philos. Mag. **3**, 1 (1927).

[68] V. Bargmann, Louis Michel, and V. L. Telegdi, Precession of the Polarization of Particles Moving in a Homogeneous Electromagnetic Field, Phys. Rev. Lett. **2**, 435 (1959).

[69] M. W. Walser, D. J. Urbach, K. Z. Hatsagortsyan, S. X. Hu, and C. H. Keitel, Spin and radiation in intense laser fields, Phys. Rev. A **65**, 043410 (2002).

[70] Yousef I. Salamin and Christoph H. Keitel, Electron Acceleration by a Tightly Focused Laser Beam, Phys. Rev. Lett. **88**, 095005 (2002).

[71] B. Gonzalez-Izquierdo, R. J. Gray, M. King, R. Wilson, R. J. Dance, H. Powell, D. A. MacLellan, J. McCreadie, N. M. H. Butler, S. Hawkes, J. S. Green, C. D. Murphy, L. C. Stockhausen, D. C. Carroll, N. Booth, G. G. Scott, M. Borghesi, D. Neely, and P. McKenna, Influence of laser polarization on collective electron dynamics in ultraintense laser–foil interactions, High Power Laser Sci. Eng. **3**, e3 (2016).

[72] G. C. Rodrigues and J. R. Duflou, Theoretical and experimental aspects of laser cutting with elliptically polarized laser beams, J. Mater. Process. Tech. **264**, 448 (2019).

[73] W. P. Leemans, A. J. Gonsalves, H.-S. Mao, K. Nakamura, C. Benedetti, C. B. Schroeder, Cs. Tóth, J. Daniels, D. E. Mittelberger, S. S. Bulanov, J.-L. Vay, C. G. R. Geddes, and E. Esarey, Multi-GeV Electron Beams from Capillary-discharge-guided Subpetawatt Laser Pulses in the Self-trapping Regime, Phys. Rev. Lett. **113**, 245002 (2014).

[74] A. J. Gonsalves *et al.*, Petawatt Laser Guiding and Electron Beam Acceleration to 8 GeV in a Laser-heated Capillary Discharge Waveguide, Phys. Rev. Lett. **122**, 084801 (2019).

[75] S. Cipiccia *et al.*, Gamma-rays from harmonically resonant betatron oscillations in a plasma wake, Nat. Phys. **7**, 867 (2011).

[76] K. T. Phuoc, S. Corde, C. Thaury, V. Malka, A. Tafzi, J. P. Goddet, R. C. Shah, S. Sebban, and A. Rousse, All-optical compton gamma-ray source, Nat. Photon. **6**, 308 (2012).

[77] M. Placidi and R. Rossmanith, e^+e^- polarimetry at LEP, Nucl. Instrum. Methods Phys. Res., Sect. A **274**, 79 (1989).